Selective synthesis and shape-dependent microwave electromagnetic properties of polymorphous ZnO complex architectures

Fangfang Du, Guoxiu Tong,[a] Chaoli Tong, and Yun Liu
Chemical Department, College of Chemistry and Life Sciences, Zhejiang Normal University, Jinhua 321004, People's Republic of China

Jianqing Tao[b]
State Key Laboratory of Advanced Technology for Materials Synthesis and Processing, Wuhan University of Technology, Wuhan 430070, People's Republic of China

(Received 9 October 2013; accepted 24 January 2014)

A simple one-pot hydrothermal approach that allowed the selective synthesis of complex ZnO architectures with varying configurations without using any surfactants and/or solid templates is proposed in this paper. The ZnO configurations include spherical aggregates, nanosheet-based flowers, microrod-composed flowers, and nanopetal-built flowers. Kinetic factors (i.e., the base type and base/Zn^{2+} molar ratio) can be easily utilized to control the oriented attachment and growth of $[Zn(OH)]^{2-}$ on the (001) polar planes, thereby regulating the morphology of ZnO architectures. The ZnO architectures were characterized by scanning electron microscopy, transmission electron microscopy, selected-area electron diffraction, x-ray diffraction, and specific surface area. The relationships between the structures and microwave electromagnetic properties were established. Enhanced dielectric and absorption properties were exhibited by ZnO flowers composed of large-aspect-ratio microrods. Such properties could be attributed to the improved microcurrent attenuation and interface scattering rather than the dielectric relaxation and microantenna radiation. This study provides a guide for creating and synthesizing highly efficient microwave absorbing materials.

I. INTRODUCTION

With the rapid development of science and technology, all kinds of electrical and electronic devices (e.g., mobile phone, local area network, radar systems, etc.) have been widely used. The abundance of these electronic devices has resulted in increasingly serious problems of electromagnetic (EM) interference.[1–3] Thus, numerous studies have currently focused on EM wave absorbing materials because they can effectively absorb EM wave by converting EM energy into heat or interference. To date, various absorbents (i.e., magnetic metals[4] and ferrite[5]) have been studied. However, these absorbents present disadvantages such as high density, narrow bandwidth, and low absorptivity, which limit their extensive applications.

ZnO nanomaterials are considered promising microwave absorption materials in civilian and military applications because of their light weight, low cost, simple synthesis, light color, and strong absorption ability.[6] ZnO is a dielectric loss medium. A normal dipole moment and spontaneous polarization along the *c*-axis generally originate from the oppositely charged ions, producing positively charged (001) Zn-polar and negatively charged (00$\bar{1}$) O-polar surfaces.[7] Additionally, the relaxation polarization and loss can also form via a back and forth migration of the electrons from polar planes or oxygen vacancies under an alternating EM field.[8] To date, most of the investigations on microwave-absorbing behavior mainly focus on nanocombs,[9] nanotetraneedle ZnO,[10] nanotrees, nanorods, dendritic nanostructures,[11] nanowires,[12] and net-like structures.[13] For example, Zhuo et al.[9] reported that the strong absorption of the ZnO nanocomb composite reached −12 dB at 11 GHz with a thickness of 2.5 mm. Cao et al.[14] found that the microwave attenuation of the cage-like ZnO/silica nanocomposites with a weight ratio of 20% was as high as −10.68 dB at the frequency of 12.79 GHz. Li et al.[13] investigated the microwave absorption property of crossed ZnO net-like micro/nanostructures and found that the value of minimum reflection loss was −37 dB at 6.2 GHz with a thickness of 4.0 mm. However, these ZnO nanomaterials were mainly synthesized by metal-vapor deposition, which requires a large amount of energy. Only a few studies have analyzed the flower-like nano/microstructures obtained through a simple and energy efficient hydrothermal process.

In this study, we developed an easy one-pot hydrothermal approach without any template or organic additive for the selective preparation of flower-like ZnO nano/microstructures. Morphological variations of the resulting products were facilitated by changing only

Address all correspondence to these authors.
[a]e-mail: tonggx@zjnu.cn
[b]e-mail: taojq@whut.edu.cn
DOI: 10.1557/jmr.2014.27

https://doi.org/10.1557/jmr.2014.27 Published online by Cambridge University Press

 © Materials Research Society 2014

the base type and base/Zn^{2+} molar ratio. The shape-dependent microwave-absorbing properties of complex ZnO nano/microstructures were also systematically investigated.

II. EXPERIMENTAL

A. Preparation

All chemicals were obtained from Sinopharm Chemical Reagent Co., Ltd. (Shanghai, P.R. China). All were of analytical grade and used as received without any further purification.

Polymorphic ZnO samples were prepared by a hydrothermal process. Typically, 0.952 g of zinc nitrate and 0.128 g of NaOH were mixed with 80 mL of deionized water. The entire mixture was placed in a 100 mL Teflon stainless autoclave and tightly sealed. The hydrothermal reaction was performed at 120 °C for 2.0 h. After that, the precipitate was filtered, washed with deionized water, and dried at 80 °C for 8 h. Morphological modulation of the ZnO products was achieved by changing only the base/Zn^{2+} molar ratio (α = 1.0 and 3.0) and base type (NaOH, ethanediamine [$C_2H_8N_2$, en], $NH_3{\cdot}H_2O$).

B. Characterization

The surface morphologies of the as-prepared samples were observed by a field-emission scanning electron microscope (Hitachi S-4800, Hitachi, Japan), operated at 10.0 kV. The transmission electron microscope (TEM) images and the corresponding selected-area electron diffraction (SAED) pattern were captured on JEM-2100F TEM (JEOL, Tokyo, Japan) operating at 200 kV. The phase analysis of the samples was performed by an x-ray diffraction (XRD; Model D/MAX-RB, Rigaku, Tokyo, Japan), with Cu K_α radiation with 2θ from 10° to 70°. The Brunauer-Emmer-Teller (BET) specific surface area (S_{BET}) was measured using a surface area analyzer (Autosorb-1, Quantachrome Co., Syosset, NY).

C. Measurement of EM parameters

Using the coaxial line method, the relative complex permittivity ($\varepsilon = \varepsilon' - j\varepsilon''$) of the sample–wax composites was tested through an Agilent N5230 vector network analyzer system (Agilent, Santa Clara, CA). The cylindrical toroidal samples with 3.0 mm of inner diameter, 7.0 mm of outer diameter, and a thickness of about 3.5 mm were prepared by uniformly mixing wax with the absorbents in various mass fractions of 20–60% and then pressed into cylindrical compacts. Reflection loss (R_L) represents the microwave absorption property and can be calculated from the relative permeability and permittivity at a given frequency (f) and coating thickness (d) using the following equations[2]:

$$R_L(\mathrm{dB}) = 20\log_{10}|(Z_{in} - Z_0)/(Z_{in} + Z_0)| \quad , \qquad (1)$$

$$Z_{in} = Z_0\sqrt{\mu/\varepsilon}\tan h\left[j(2\pi fd/c)\sqrt{\mu/\varepsilon}\right] \quad , \qquad (2)$$

$$Z_0 = \sqrt{\mu_0/\varepsilon_0} \quad , \qquad (3)$$

where c is the light velocity, Z_0 is the characteristic impedance of free space, and Z_{in} is the input impedance between the free space and the materials.

III. RESULTS AND DISCUSSION

A. Results from SEM and TEM

SEM, TEM, and SAED were used to reveal the influence of the base/Zn^{2+} molar ratio and base type on the surface morphologies and microstructures of the samples. As shown in Fig. 1(a), using NaOH as base with α = 1.0, the as-prepared products were 0.5- to 1.0-μm diameter microspheres consisting of nanoparticles with several tens of nanometers in size. When α was increased to 3.0, the products were monodispersed and uniform microspheres were formed with a diameter ranging from 4 to 5 μm [Fig. 1(b)]. These microspheres were composed of numerous densely arranged nanosheets that radially spread and formed well-defined flower-like architectures. Periodical lattice stripes can be observed in almost the whole HRTEM visual field [Fig. 1(e)]. The crystal plane distance was measured with a length of 0.52 nm, which corresponded to the [001] direction of ZnO. The strong and clear diffuse spots in the SAED pattern [inset in Fig. 1(e)] illustrate the single crystal nanosheets.

When en was used at an en/Zn^{2+} molar ratio of 1.0, the hydrothermal precipitates formed a radial structure with microrods projected outwards, exhibiting a flower-like configuration [Fig. 1(c)]. The diameters of the flowers ranged from 8.0 to 10.0 μm. These microrods had aspect ratios of approximately 5.0, and their diameters slightly decreased from 1.0 μm on the body to approximately 600 nm at the tip. The sharp diffraction spots in the SAED pattern [inset of Fig. 1(f)], taken from individual ZnO microrods [Fig. 1(f)], further demonstrated that the [001] direction was the preferred growth direction of crystal formation with a perfect single crystalline nature.

Substituting NaOH with $NH_3{\cdot}H_2O$ still resulted in the flower-like shape of the ZnO samples, with diameters of about 1.0 μm to 1.5 μm [Figs. 1(d) and 1(g)]. Each flower comprised several petals approximately 1.0 in aspect ratio, radially projecting from one center. The surfaces of the ZnO flowers were not smooth and covered by large amounts of nanoparticles. The irregular SAED pattern in the inset of Fig. 1(g) indicated the polycrystalline nature of the nanopetal and the existence of shear defects. We showed in our previous study[6,7] that the initially formed nanoparticles can rapidly grow preferentially along the [001] direction and subsequently act as "pioneer crystals" to direct the

https://doi.org/10.1557/jmr.2014.27 Published online by Cambridge University Press

formation of the nanopetals. The nanoparticles that grew on the nanopetal surface eventually remained parallel to the [001] direction by rotating under hydrothermal conditions. In the present study, the growth of the flower-like ZnO architectures was due to the polar surface-induced oriented attachment growth. When various bases and base/Zn^{2+} molar ratios were introduced to the reaction system, different coordination agents react with Zn^{2+} ions to form zinc coordination compounds with various unstable constant values. These variations affected the attachment and growth behavior of $[Zn(OH)_4]^{2-}$ on the (001) polar planes as well as the nucleation and growth rates of ZnO nanocrystals.[6,7,15]

B. XRD analysis

XRD was used to further study the effects of the base/Zn^{2+} molar ratio and base type on phase structure, intensity ratio of $I_{(100)}/I_{(002)}$, crystal size, and internal strain of the products. The XRD patterns in Fig. 2(a) showed that all peaks can be indexed to the hexagonal ZnO with wurtzite structure (space group $P6_3mc$; a = 3.2498 Å, c = 5.2066 Å; JCPDS 36-1451). No characteristic impurity

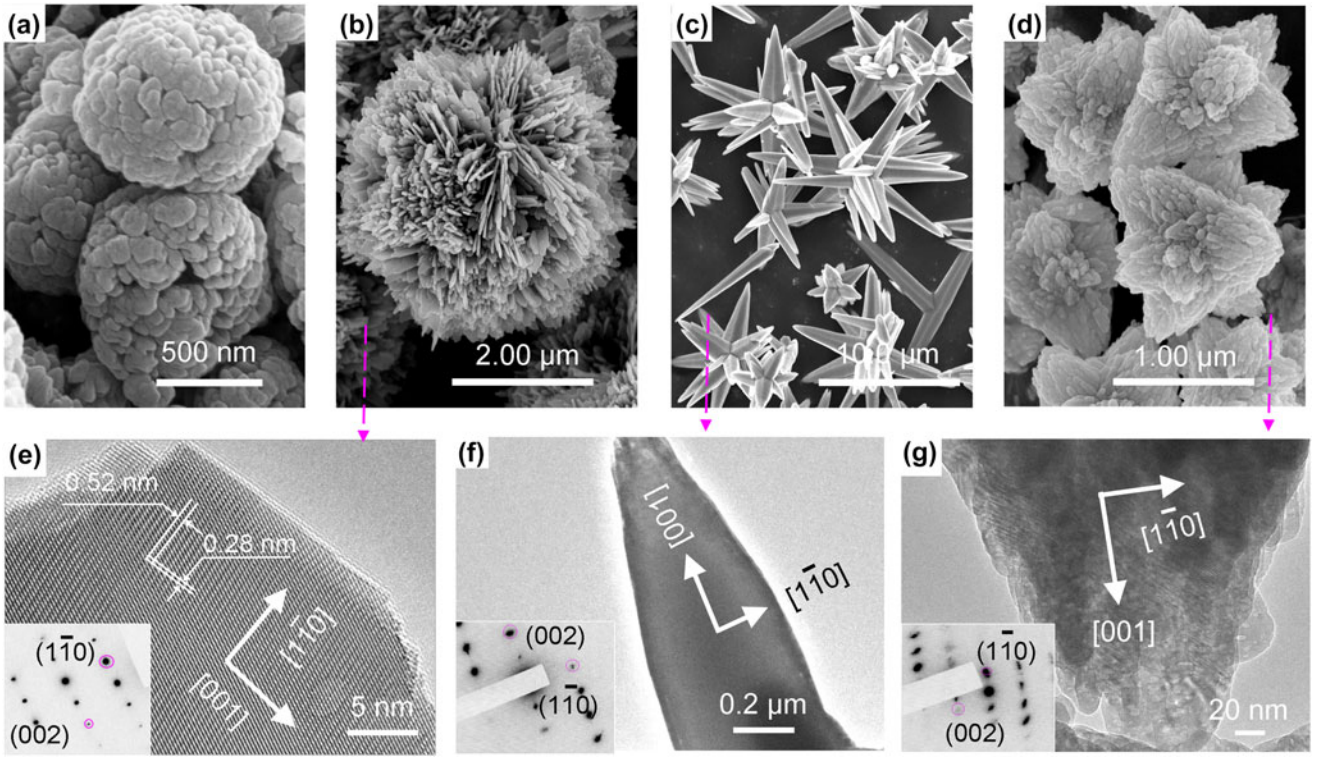


FIG. 1. (a–d) SEM and (e–g) TEM images of polymorphous ZnO samples produced at various base/Zn^{2+} molar ratios (α) and base types. (a) Spherical aggregates, α = 1.0 (NaOH/Zn^{2+}); (b and e) nanosheet-based flowers, α =3.0 (NaOH/Zn^{2+}); (c and f) microrod-composed flowers, α =1.0 (en/Zn^{2+}); and (d and g) nanopetal-built flowers, α = 2.0 ($NH_3{\cdot}H_2O$/Zn^{2+}). The insets in e, f, and g are the corresponding SAED patterns.

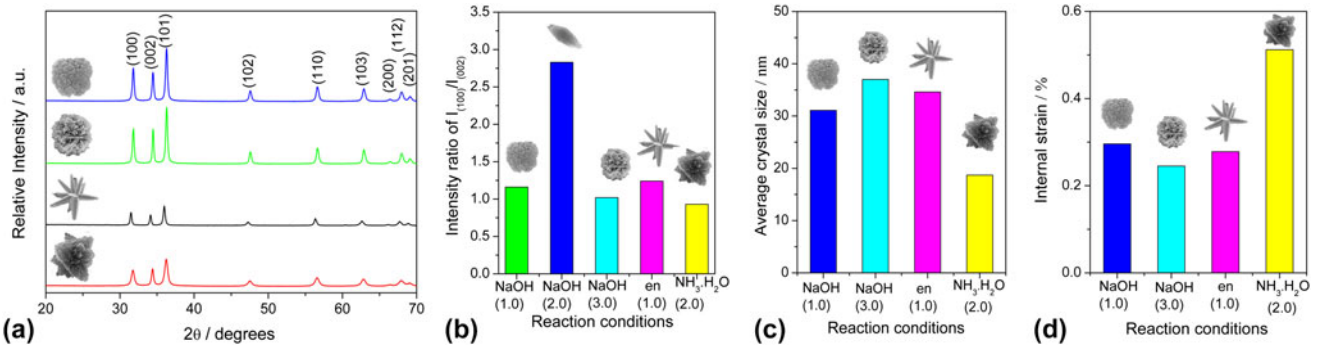


FIG. 2. (a) XRD patterns, (b) intensity ratio of $I_{(100)}/I_{(002)}$, (c) average crystal size, and (d) internal strain of polymorphous ZnO samples formed at various base/Zn^{2+} molar ratios (α) and base types.

https://doi.org/10.1557/jmr.2014.27 Published online by Cambridge University Press

peaks, such as $ZnCO_3{\cdot}2Zn(OH)_2{\cdot}H_2O$, were observed, indicating that all samples were pure ZnO phases. However, the change in the α and base types initiated an increase in intensities of all diffraction peaks at various degrees. This phenomenon is generally related to the enhanced crystallization, formation of large crystallites, or well-ordered orientation.[16] From Fig. 2(b), NaOH displayed the highest intensity ratio of $I_{(100)}/I_{(002)}$ among the bases used in this study while keeping the stoichiometric ratio of Zn^{2+} to OH^- unchanged (i.e., at 2.0). With NaOH as base, the intensity ratio of $I_{(100)}/I_{(002)}$ peaked at $\alpha = 2.0$. In general, a small $I_{(100)}/I_{(002)}$ ratio corresponds to an intense (002) peak, indicating the preferential growth of rods along the *c*-axis with (001) or (00$\bar{1}$) end faces. Conversely, a very large $I_{(100)}/I_{(002)}$ ratio indicated the prior growth of rods along the *a*-axis ([100] direction).[17] Such variations implied that changing bases and base/Zn^{2+} molar ratios (α) could modulate the growth direction of ZnO nanocrystals. The average crystallite sizes and the internal strain of the samples were determined according to the Hall–Williamson equation: $\beta\cos\theta = \frac{K\lambda}{\delta} + 2\varepsilon sin\theta$, where β is the full width at half-maximum (FWHM) of the samples, λ is the x-ray wave length used, δ is the grain size, *K* is Scherrer constant, ε is the internal strain, and θ is Bragg angle. β can be given as $\beta^2 = \beta^2_{exp} - \beta^2_{inst}$, where β_{inst} is the FWHM of the Si powder used for calibration and β_{exp} is the evaluated FWHM. Figures 2(c)and 2(d) show that microrod- and nanosheet-based flowers had larger crystal size and lower internal strain than spherical aggregates and nanopetal-built flowers. The data indicated that increasing α and using en or NaOH as the base enhanced crystal size and crystallinity.

C. BET study

In addition to the morphological and structural modulation, base/Zn^{2+} molar ratio and base type also considerably influenced the specific surface area (S_{BET}) of the products. The BET S_{BET} was determined by a multipoint BET method using the adsorption data in a relative pressure (P/P_0) range from 0.05 to 0.25. Figure 3 shows that the S_{BET} of the spherical aggregates was as large as 15.60 m^2/g, which was much higher than those of nanosheet-based-flowers (11.60 m^2/g), microrod-composed flowers (1.68 m^2/g), and nanopetal-built flowers (7.73 m^2/g). The difference was mainly ascribed to the mode of assembly and crystal size of nanocrystals.

D. Dielectric properties

Figure 4 showed the frequency dependence of the relative complex permittivity and dielectric loss for the wax-composites containing the various mass fractions and morphologies of ZnO. As shown in Figs. 4(a)–4(c), the ε′, ε″, and tan δ_E values of the nanosheet-built flowers fluctuated within small ranges of 2.1–3.4, 0–0.5, and 0–0.17,

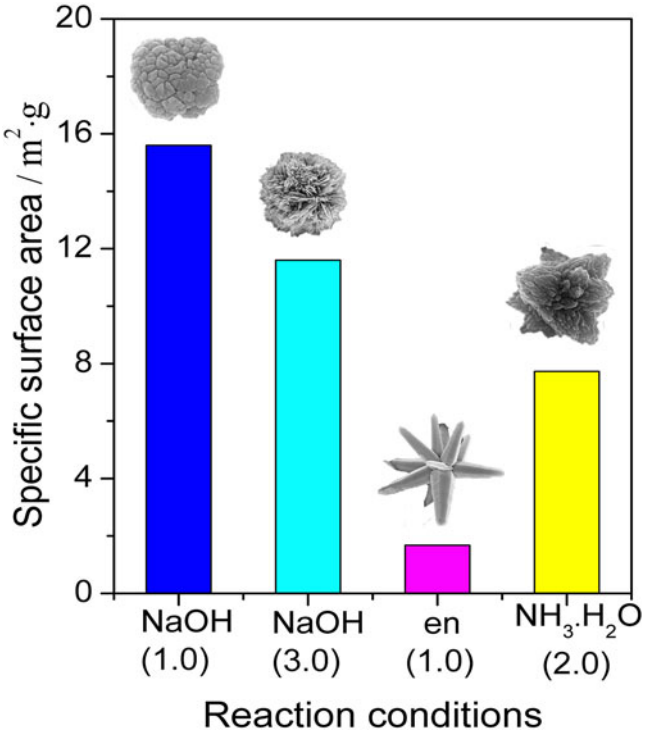


FIG. 3. Specific surface area (S_{BET}) of the samples obtained at the various base/Zn^{2+} molar ratios (α) and bases.

respectively. As the mass fraction increased, the ε′ value gradually increased; the ε″ and tan δ_E values also showed less variation from 20 to 40% with a steep increase at 60%. This sharp variation may be related to the formation of the percolation semiconductive network in the matrix under a high mass fraction.[18] Contrastive analysis (Fig. 4) revealed that the ε′, ε″, and tan δ_E values of nanosheet-built flowers were almost as same as those of the spherical aggregates and nanopetal-composed flowers and conspicuously lower than those of microrod-based flowers. Thus, the flowers composed by high aspect ratio microrods had a higher capacity for storage and loss of electrical energy.

The microwave responses of complex nano/microstructures are usually associated with dielectric relaxation, microcurrent attenuation, interface scattering, and microantenna radiation.[19] First, the dielectric relaxation is a result of the orientation, interfacial, atomic, and space charge polarizations. These types of polarizations strongly depend on the material shapes and microstructures. ZnO is considered as a dielectric loss medium, and its dielectric relaxation is usually related to the characteristic of its polar surfaces. The ZnO polar monomer contains oppositely charged ions. The positively charged (001) Zn-polar and negatively charged (00$\bar{1}$) O-polar surfaces generate a normal dipole moment and spontaneous polarization along the *c* axis. Under an alternating EM field, the electrons from the polar planes or oxygen vacancies migrate back and forth to form relaxation polarization and loss, respectively.[8]

https://doi.org/10.1557/jmr.2014.27 Published online by Cambridge University Press

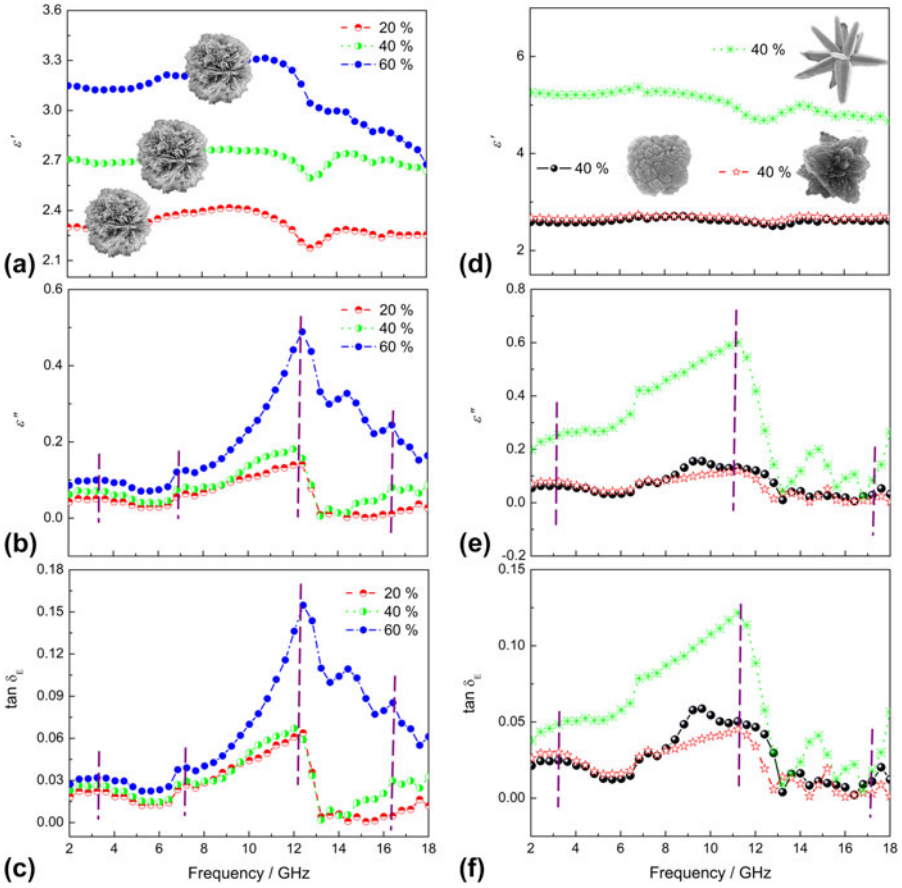


FIG. 4. Frequency dependence of the real (ε′) and imaginary (ε″) parts of the complex permittivity and the dielectric loss (tan $\delta_E = \varepsilon''/\varepsilon'$) for the ZnO wax composites: (a–c) various mass fractions of the nanosheet-built flowers and (d) 40% ZnO spherical aggregates, (e) microrod-composed flowers, and (f) nanopetal-built flowers.

According to our previous studies,[20] the increased ε′, ε″, and tan δ_E values were due to the enhancement of space charge polarization from the increasing defects, interface polarization from increasing surface area, or orientation polarization from significantly increasing aspect ratio. Thus, the ZnO samples with large S_{BET} and high internal strain (corresponding to high defects) should display large ε′, ε″, and tan δ_E values. But this was not observed in the permittivity of nanopetal-built flowers and spherical aggregates. Therefore, it can be inferred that the orientation polarization from the significantly increasing aspect ratio is one of the crucial factors for the enhanced permittivity of the microrod-based flowers.

Second, continuous semiconductive micronetworks in the matrix may induce large-scale vibrating microcurrent attenuation when the EM wave travels into the ZnO wax composites. The mass fraction and shape of the ZnO particles are the two key factors in the formation of the nets. Compared with the nanosheet-built flowers, spherical aggregates, and nanopetal-built flowers, the microrod-based flowers with the large aspect ratio are more prone to form such nets in the matrix by linking with one another at a low mass fraction. The nets can also form by elevating the mass fraction of the ZnO particles within certain limits. Flower-like architectures randomly distributed in the matrix can also generate multiple interface scattering and further increase the attenuation of the EM wave. The multiple interface scattering strengthens as the mass fraction and the interface increase.

Third and last, discontinuous flower-like architectures can act as isotropic quasi-antennas, which produce microantenna radiation. The behavior induces EM energy into becoming a dissipative current. With the increasing mass fraction, the discontinuous flower-like architectures decrease and the continuous micronetworks gradually form. Thus, the former decreases the microantenna radiation and the latter enhances the microcurrent attenuation. Overall, increasing mass fraction from 20 to 40% leads to the similar permittivity, as a result of the cooperative effect of the reduced microantenna radiation, the increased interface scattering and dielectric relaxation. However, steeply increased permittivity in the high mass fraction and shape of ZnO microrod-based flowers results from the microcurrent attenuation and interface scattering.

https://doi.org/10.1557/jmr.2014.27 Published online by Cambridge University Press

The ε'' and tan δ_E plots presented highly complex nonlinear resonant behaviors relative to the EM energy loss, with a strong and wide peak over 10–14 GHz but low resonant peaks of 2–5, 6–8, and 16–18 GHz. Similar multiresonance behaviors have been found in ZnO nanocombs,[9] ZnO dendritic nanostructures,[11] nanotrees,[21] and micro/nanorod networks,[13] which were generally associated with highly conductive and skin effects,[22] electronic spin and charge polarizations caused by point effects, and polarized centers.[23,24] In the present study, two weak resonant peaks at 6–8 and 16–18 GHz were derived from microantenna radiation, whereas a strong wide peak at approximately 12 GHz was caused by the cooperative action of interface scattering, microcurrent attenuation, and dielectric relaxation.[19] Obviously, a strong resonance peak usually corresponded to a strong reflection loss, which was exhibited by high mass fraction and/or the shape of microrod-composed flowers (Fig. 4).

E. Microwave absorption properties

Figure 5 shows the R_L curves of the wax composites containing the flower-like ZnO powders with various mass ratios and morphologies. Several evident resonance absorbing peaks were observed on all R_L plots of the ZnO wax composites including 20 wt% nanosheet-built ZnO flowers [Fig. 5(a)]. A strong and broad peak was located at 11.0 GHz and two weak ones were situated at approximately 3.0 and 17.0 GHz, respectively. As the sample thickness increased from 1.0 to 6.0 mm, the intensities of three absorption peaks gradually increased and their positions remained almost the same (i.e., no movement to lower frequencies). The nesting absorption

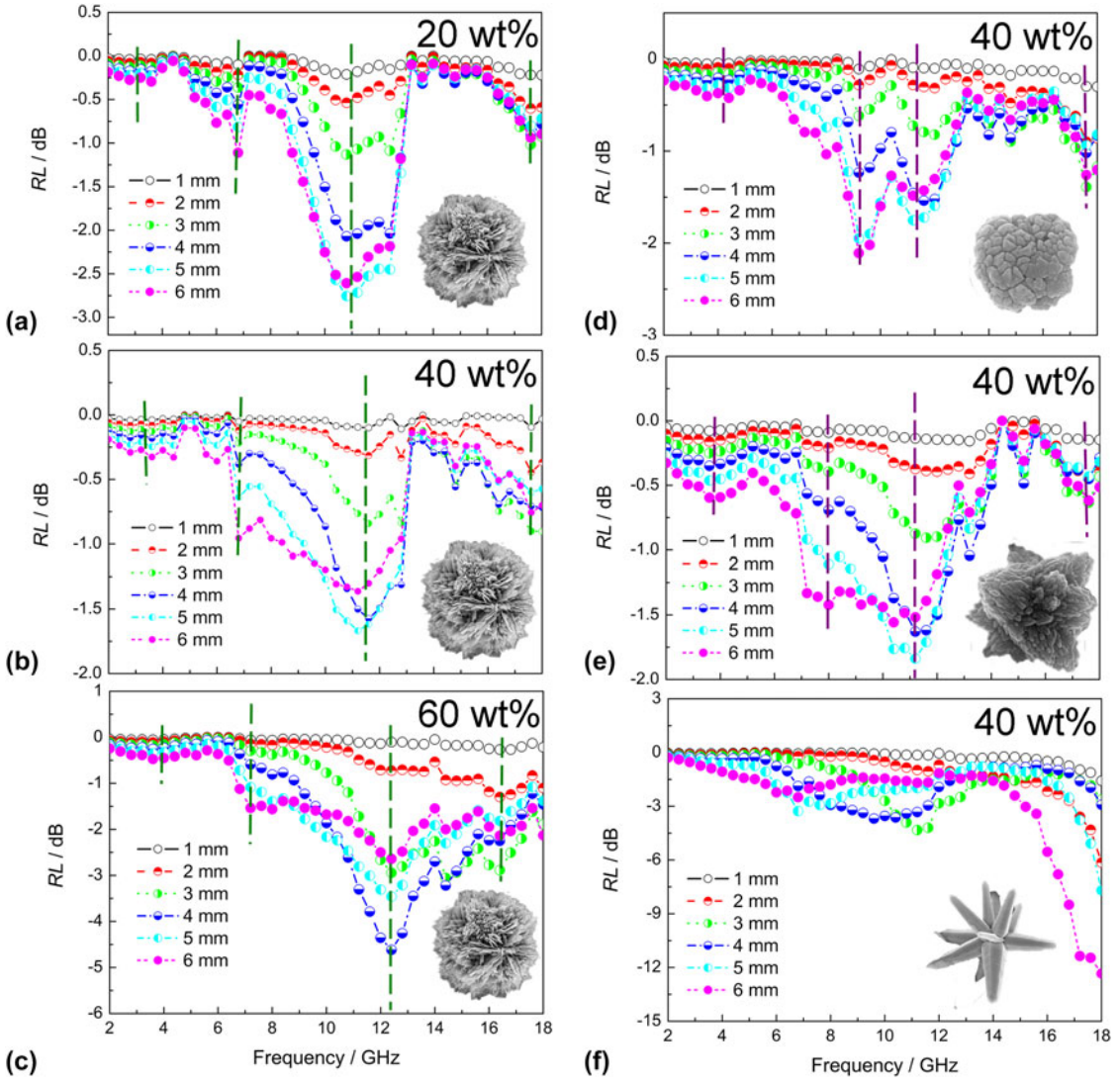


FIG. 5. Reflection loss curves for the ZnO wax composites including various mass fractions and morphologies of ZnO powders. (a–c) Various mass fractions of the nanosheet-built ZnO flowers and (d) 40% ZnO spherical aggregates, (e) nanopetal-built flowers, and (f) microrod-composed flowers.

https://doi.org/10.1557/jmr.2014.27 Published online by Cambridge University Press

peaks also still existed not only at 40 and 60 wt% [Figs. 5(a)–5(c)] but also in spherical aggregates and nanopetal-built flowers [Figs. 5(d)–5(f)]. The peaks gradually broadened and their positions slightly moved to a higher frequency with the increased mass fraction [Figs. 5(a)–5(c)].

A similar phenomenon has been reported in spherical Co, hollow Co nanochains, and MWCNTs/ZnO samples, which were ascribed to the effect of dual nonlinear dielectric resonance and negative permeability[25] or the resonant behavior caused by interface and skin effect.[25] In our previous studies, urchin-like Fe_2O_3 took on a nesting absorption peak at approximately 16.5 GHz.[26] Three nesting absorbing peaks at approximately 12.5, 14.8, and 16.5 GHz can be observed in flower-like Co superstructures, originating from frequency-selective surface-absorption properties.[27] The present data showed that the positions of multiresonance absorbing peaks were unexpectedly similar to the resonance peaks on ε'' and tan δ_E plots. This result indicated that the microwave absorption of ZnO flowers originated from the multiresonance loss. By contrast, the absorption peaks of microrod-composed flowers did not remain at a stable frequency but gradually moved to lower frequencies with increased coating thickness. The change is due to the resonant absorption caused by the quarter-wave length attenuation when the reflected waves and incident waves meet in a material.[28] Compared with dielectric relaxation and microantenna radiation, microcurrent attenuation and interface scattering are highly important microwave responses for improving the dielectric and microwave absorption properties of ZnO architectures. Obviously, a flower-like architecture built by large aspect ratio microrods is a promising configuration for designing novel microwave absorbing materials.

IV. CONCLUSION

In summary, various ZnO architectures, including spherical aggregates and flowers (composed by nanosheets, microrods, and nanopetals), have been synthesized by an easy one-pot hydrothermal approach in the absence of any template or organic additive. The morphology and structure of ZnO architectures were easily manipulated by merely changing the base type and the molar ratio of base to Zn^{2+} (α). Compared with dielectric relaxation and microantenna radiation, microcurrent attenuation and interface scattering are more important microwave responses for improving the dielectric and microwave absorption properties of the ZnO architectures. Several stable nesting absorption peaks were exhibited by nanosheet-built flowers, spherical aggregates, and nanopetal-built flowers because of multiresonance loss. However, flowers built by large-aspect-ratio microrods present enhanced absorption peaks because of the quarter-wave length attenuation, and thus is a promising configuration for designing novel microwave-absorbing materials.

ACKNOWLEDGMENTS

This work was financially supported by the Natural Scientific Foundation of China (51102215), Chinese Scholarship Council (201208330114), Natural Scientific Foundation of Zhejiang Province (Y4100022), Teacher Training Project of Zhejiang Normal University (KYJ06Y12134), and National Innovation and Entrepreneurship Training Program of Undergraduates (201310345016).

REFERENCES

1. G.X. Tong, J.G. Guan, Z.D. Xiao, F.Z. Mou, W. Wang, and G.Q. Yan: In situ generated H_2 bubble-engaged assembly: A one-step approach for shape-controlled growth of Fe nanostructures. *Chem. Mater.* **20**, 3535–3539 (2008).
2. G.X. Tong, Q. Hu, W.H. Wu, W. Li, H.S. Qian, and Y. Liang: Submicrometer-sized NiO octahedra: Facile one-pot solid synthesis, formation mechanism, and chemical conversion into Ni octahedra with excellent microwave-absorbing properties. *J. Mater. Chem.* **22**, 17494–17504 (2012).
3. X.A. Fan, J.G. Guan, Z.Z. Li, F.Z. Mou, G.X. Tong, and W. Wang: One-pot low temperature solution synthesis, magnetic and microwave electromagnetic properties of single-crystal iron submicron cubes. *J. Mater. Chem.* **20**, 1676–1682 (2010).
4. G-X. Tong, W-H. Wu, Q. Hu, J-H. Yuan, and H-S. Qian: Enhanced electromagnetic characteristics of porous iron particles made by a facile corrosion technique. *Mater. Chem. Phys.* **132**, 563–569 (2012).
5. G.X. Tong, W.H. Wu, R. Qiao, J.H. Yuan, J.G. Guan, and H.S. Qian: Morphology dependence of static magnetic and microwave electromagnetic characteristics of polymorphic Fe_3O_4 nanomaterials. *J. Mater. Res.* **26**, 1639–1645 (2011).
6. Q. Hu, G.X. Tong, W.H. Wu, F.T. Liu, H.S. Qian, J.G. Guan, and D.Y. Hong: Selective preparation and novel microwave electromagnetic characteristics of polymorphous ZnO architectures made from a facile one-step ethanediamine (en)-assisted hydrothermal approach. *CrystEngComm* **15**, 1314–1323 (2013).
7. G-X. Tong, F-F. Du, Y. Liang, Q. Hu, R-N. Wu, J-G. Guan, and X. Hu: Polymorphous ZnO complex architectures: Selective synthesis, mechanism, surface area- and Zn-polar plane-codetermining antibacterial activity. *J. Mater. Chem. B* **1**, 454–463 (2013).
8. Y.X. Huang, Q.X. Cao, Z.M. Li, H.Q. Jiang, Y.P. Wang, and G.F. Li: Effect of synthesis atmosphere on the microwave dielectric properties of ZnO powders. *J. Am. Ceram. Soc.* **92**, 2129–2131 (2009).
9. R.F. Zhuo, H.T. Feng, Q. Liang, J.Z. Liu, J.T. Chen, D. Yan, J.J. Feng, H.J. Li, S. Cheng, B.S. Geng, X.Y. Xu, J. Wang, Z.G. Wu, P.X. Yan, and G.H. Yue: Morphology-controlled synthesis, growth mechanism, optical and microwave absorption properties of ZnO nanocombs. *J. Phys. D: Appl. Phys.* **41**, 185405 (2008).
10. J. Yuan, W-L. Song, X-Y. Fang, X-L. Shi, Z-L. Hou, and M-S. Cao: Tetra-needle zinc oxide/silica composites: High-temperature dielectric properties at X-band. *Solid State Commun.* **154**, 64 (2013).
11. R.F. Zhuo, H.T. Feng, J.T. Chen, D. Yan, J.J. Feng, H.J. Li, B.S. Geng, S. Cheng, X.Y. Xu, and P.X. Yan: Multistep synthesis, growth mechanism, optical, and microwave absorption properties of ZnO dendritic nanostructures. *J. Phys. Chem. C* **112**, 11767–11775 (2008).

https://doi.org/10.1557/jmr.2014.27 Published online by Cambridge University Press

12. Y.J. Chen, M.S. Cao, T.H. Wang, and Q. Wan: Microwave absorption properties of the ZnO nanowire-polyester composites. *Appl. Phys. Lett.* **84**, 3367–3369 (2004).
13. H.F. Li, Y.H. Huang, G.B. Sun, X.Q. Yan, Y. Yang, J. Wang, and Y. Zhang: Directed growth and microwave absorption property of crossed ZnO netlike micro-/nanostructures. *J. Phys. Chem. C* **114**, 10088–10091 (2010).
14. M-S. Cao, X-L. Shi, X-Y. Fang, H-B. Jin, Z-L. Hou, Z. Wei, and Y-J. Chen: Microwave absorption properties and mechanism of cagelike ZnO/SiO_2 nanocomposites. *Appl. Phys. Lett.* **91**, 203110 (2007).
15. Z.Q. Li, Y.J. Xiong, and Y. Xie: Selective growth of ZnO nanostructures with coordination polymers. *Nanotechnology* **16**, 2303 (2005).
16. G.X. Tong, J.G. Guan, and Q.J. Zhang: Goethite hierarchical nanostructures: Glucose-assisted synthesis, chemical conversion into hematite with excellent photocatalytic properties. *Mater. Chem. Phys.* **127**, 371–378 (2011).
17. A. Mclaren, T. Valdes-Solis, G.Q. Li, and S.C. Tsang: Shape and size effects of ZnO nanocrystals on photocatalytic activity. *J. Am. Chem. Soc.* **131**, 12540–12541 (2009).
18. G.X. Tong, W.H. Wu, Q. Hua, Y.Q. Miao, J.G. Guan, and H.S. Qian: Enhanced electromagnetic characteristics of carbon nanotubes/carbonyl iron powders complex absorbers in 2–18GHz ranges. *J. Alloys Compd.* **509**, 451–456 (2011).
19. X-Y. Fang, M-S. Cao, X-L. Shi, Z-L. Hou, W-L. Song, and J. Yuan: Microwave responses and general model of nanotetraneedle ZnO: Integration of interface scattering, microcurrent, dielectric relaxation, and microantenna. *J. Appl. Phys.* **107**, 054304 (2010).
20. G.X. Tong, J. Ma, W.H. Wu, Q. Hua, R. Qiao, and H.S. Qian: Grinding speed dependence of microstructure, conductivity, and microwave electromagnetic and absorbing characteristics of the flaked Fe particles. *J. Mater. Res.* **26**, 682–688 (2011).
21. R.F. Zhuo, L. Qiao, H.T. Feng, J.T. Chen, D. Yan, Z.G. Wu, and P.X. Yan: Microwave absorption properties and the isotropic antenna mechanism of ZnO nanotrees. *J. Appl. Phys.* **104**, 094101 (2008).
22. A.N. Langarkov and A.K. Sarychev: Electromagnetic properties of composites containing elongated conducting inclusions. *Phys. Rev. B* **53**, 6318 (1996).
23. P.C.P. Watts, W.K. Hsu, A. Barnet, and B. Chambers: High permittivity from defective multiwalled carbon nanotubes in the X-band. *Adv. Mater.* **15**, 600–603 (2003).
24. R.C. Che, L-M. Peng, X.F. Duan, Q. Chen, and X.L. Liang: Microwave absorption enhancement and complex permittivity and permeability of Fe encapsulated within carbon nanotubes. *Adv. Mater.* **16**, 401–405 (2004).
25. X.L. Shi, M.S. Cao, J. Yuan, and X.Y. Fang: Dual nonlinear dielectric resonance and nesting microwave absorption peaks of hollow cobalt nanochains composites with negative permeability. *Appl. Phys. Lett.* **95**, 163108 (2009).
26. G.X. Tong, W.H. Wu, J.G. Guan, H.S. Qian, J.H. Yuan, and W. Li: Synthesis and characterization of nanosized urchin-like α-Fe_2O_3 and Fe_3O_4: Electromagnetic properties. *J. Alloys Compd.* **509**, 4320–4326 (2011).
27. G.X. Tong, J.H. Yuan, W.H. Wu, Q. Hu, H.S. Qian, L.C. Li, and J.P. Shen: Flower-like Co superstructures: Morphology and phase evolution mechanism and novel microwave electromagnetic characteristics. *CrystEngComm* **14**, 2071–2079 (2012).
28. W.L. Song, M.S. Cao, B. Wen, Z.L. Hou, J. Cheng, and J. Yuan: Synthesis of zinc oxide particles coated multiwalled carbon nanotubes: Dielectric properties, electromagnetic interference shielding and microwave absorption. *Mater. Res. Bull.* **47**, 1747–1754 (2012).

https://doi.org/10.1557/jmr.2014.27 Published online by Cambridge University Press